

Supernova enhanced cosmic ray ionization and induced chemistry in a molecular cloud of W51C

C. Ceccarelli¹, P. Hily-Blant¹, T.Montmerle^{1,2}, G.Dubus¹, Y.Gallant³, A.Fiasson⁴

Received - ; accepted -

ABSTRACT

Cosmic rays pervade the Galaxy and are thought to be accelerated in supernova shocks. The interaction of cosmic rays with dense interstellar matter has two important effects: 1) high energy ($\gtrsim 1$ GeV) protons produce γ -rays by π^0 -meson decay; 2) low energy ($\lesssim 1$ GeV) cosmic rays (protons and electrons) ionize the gas. We present here new observations towards a molecular cloud close to the W51C supernova remnant and associated with a recently discovered TeV γ -ray source. Our observations show that the cloud ionization degree is highly enhanced, implying a cosmic ray ionization rate $\sim 10^{-15} \text{ s}^{-1}$, i.e. 100 times larger than the standard value in molecular clouds. This is consistent with the idea that the cloud is irradiated by an enhanced flux of freshly accelerated low-energy cosmic rays. In addition, the observed high cosmic ray ionization rate leads to an instability in the chemistry of the cloud, which keeps the electron fraction high, $\sim 10^{-5}$, in a large fraction ($A_V \geq 6 \text{ mag}$) of the cloud and low, $\sim 10^{-7}$, in the interior. The two states have been predicted in the literature as high- and low-ionization phases (HIP and LIP). This is the observational evidence of their simultaneous presence in a cloud.

Subject headings: ISM: abundances — ISM: molecules — —

¹UJF-Grenoble 1 / CNRS-INSU, Institut de Planétologie et d'Astrophysique de Grenoble (IPAG) UMR 5274, Grenoble, France
Cecilia.Ceccarelli@obs.ujf-grenoble.fr, Pierre.Hily-Blant@obs.ujf-grenoble.fr, Guillaume.Dubus@obs.ujf-grenoble.fr

²Institut d'Astrophysique de Paris, CNRS, France
montmerl@iap.fr

³Laboratoire de Physique Théorique et Astroparticules, UMR 5207, CNRS/IN2P3, Université Montpellier II, France
Yves.GALLANT@lpta.in2p3.fr

⁴LAPP, Laboratoire d'Annecy-le-Vieux de Physique des Particules, UMR/IN2P3-CNRS, Université de Savoie, Annecy-le-Vieux, France
fiasson@lapp.in2p3.fr

1. Introduction

Cosmic rays (CR) pervade the Galaxy. In the dense interstellar medium (ISM), they play a crucial role as they are the primary source of ionization, starting a complex chemistry which leads to hundreds molecules, and influencing the star and planet formation processes by creating ions, which in turn are coupled with the magnetic fields, this regulating gravitational collapse.

There is little doubt that CR are accelerated in the expanding shocks of supernova remnants (SNRs, e.g. Hillas 2005; Caprioli et al. 2011). High energy ($\gtrsim 1$ GeV) CR (mainly protons) interact with hydrogen atoms and produce γ rays via π^0 decay (Hayakawa 1952; Stecker 1971). In this case, the predicted γ -ray luminosity L_γ is proportional to the π^0 -decay γ -ray emissivity, which depends on the local CR density, and to the irradiated molecular cloud mass (e.g. Aharonian & Atoyan 1996). Hence, giant molecular clouds close to, or even better, penetrated by SNRs can be bright γ -ray sources. Conversely, molecular clouds associated with bright γ -ray sources can probe enhanced CR densities. Several CR interaction sites have now been tentatively identified with the latest generation of GeV/TeV observatories (e.g. Montmerle 2010). The main difficulty remains to distinguish between emission from proton and/or bremsstrahlung or inverse Compton from electrons. Even in well-documented cases such as IC443 (Albert et al. 2007) and W28 (Aharonian et al. 2008) SNRs, the GeV-TeV emission mechanism remains unclear. In other cases (in particular for W51C; Abdo et al. 2009; Feinstein et al. 2009) π^0 -decay appears to be the dominant γ -ray emission mechanism. In these cases, the derived local relativistic proton density is very high, typically one to two orders of magnitude higher than the average galactic CR density. Such high densities should also have visible effects at lower CR energies ($\lesssim 1$ GeV), in the regime where CR ionize molecular clouds (e.g. Kamae et al. 2006; Gabici et al. 2009; Padovani et al. 2009; Fatuzzo et al. 2010).

We propose that the physical interaction between SN-accelerated energetic particles and molecular gas, where an association is suggested by the presence of a γ -ray source, can be demonstrated by using the impact of low-energy CR on the cloud chemistry. The method is based on the determination of the ionization degree of the molecular cloud, which in turn gives a measure of the CR ionization rate ζ (to be compared with the “standard” value $\zeta_0 \sim 10^{-17} \text{ s}^{-1}$ for dense clouds; Glassgold & Langer 1974). In dense gas, the ionization can be obtained by measurements of the $\text{DCO}^+/\text{HCO}^+$ abundance ratio (e.g. Guélin et al. 1977). Briefly, HCO^+ and DCO^+ are formed by the reaction of CO with H_3^+ and H_2D^+ respectively: $\text{CO} + \text{H}_3^+ \rightarrow \text{HCO}^+ + \text{H}_2$ and $\text{CO} + \text{H}_2\text{D}^+ \rightarrow \text{DCO}^+ + \text{H}_2$. Consequently, the $\text{DCO}^+/\text{HCO}^+$ ratio directly depends on the $\text{H}_2\text{D}^+/\text{H}_3^+$ only. In molecular clouds, CR ionize the gas by ionizing H and H_2 at a rate ζ and forming the molecular ion H_3^+ , whereas H_2D^+ is

formed by the reaction of H_3^+ with HD. Since both molecules are destroyed by the reaction with the most abundant neutral species, CO, and by the recombination with electrons, the $\text{DCO}^+/\text{HCO}^+$ ratio is an almost direct measure of the gas ionization degree. The method has been extensively applied to derive the ionization degree of molecular clouds and dense cores. The measured values range between 1×10^{-8} and 1×10^{-6} , depending on the gas density, leading to estimates of ζ between 10^{-18} and 10^{-16} s^{-1} (Caselli et al. 1998: hereinafter CWTH98). Finally, Indriolo et al (2010) recently reported line absorption observations of H_3^+ , measuring the ionization in the *diffuse gas* of the outer parts of the cloud associated with IC443. Their measurements indicate values of ζ only five times larger than the average in diffuse clouds. In this Letter, we report observations of the $\text{DCO}^+/\text{HCO}^+$ ratio towards the *dense gas* of a cloud interacting with the SNR W51C.

2. W51C, a SNR interacting with a molecular cloud

W51C (also known as J1923+141 and G49.2-0.7 in the literature) is a well known SNR at a distance of $\sim 6 \text{ kpc}$ (Kundu & Velusamy 1967). The SNR extends about $30'$ (equivalent to $\sim 60 \text{ pc}$), is about $3 \times 10^4 \text{ yrs}$ old (Koo et al. 1995) and is associated with a molecular cloud, engulfed by the blast wave, whose mass is $10^4 M_\odot$ and average density $\sim 10 \text{ cm}^{-3}$ (Koo & Moon 1997). Five HII regions lie at the border of the SNR, the W51A and B star forming regions. Observations of HI and CO line emission have shown the presence of shocked material north-west, at about a distance of 10 pc from the center of the SNR (Koo et al. 1995; 1997), where OH maser emission is also detected (Hewitt et al. 2008). In this work, we targeted five positions of the molecular cloud (Table 1). Four of them lie a few arcmin away from the shocked region, while one (point A) lies at the northern edge of it. An extended ($\sim 28 \text{ pc}$) GeV–TeV source has been detected by HESS (Feinstein et al. 2009) and Fermi-LAT (Abdo et al. 2009), with a total γ -ray luminosity of $\sim 10^{36} \text{ erg s}^{-1} \text{ cm}^{-2}$ (Abdo et al. 2009), making W51C one of the most luminous γ -ray sources of our Galaxy. Based on the observed GeV–TeV γ -ray spectrum, Abdo et al. (2010) claim that almost 99% of the observed γ -rays is due to the decay of π^0 mesons produced in inelastic collisions between accelerated protons and target gas.

3. Observations and results

We observed five positions roughly sampling the cloud overlapping the HESS emission (§2; Tab. 1). To constrain the gas physical conditions, we observed the ^{13}CO and C^{18}O 1–0 and 2–1 transitions, while to measure the ionization degree, we observed the H^{13}CO^+ 1–0

and DCO^+ 2–1 transitions. The observations were obtained using the APEX and IRAM-30m telescopes (Tab. 1). The amplitude calibration was done typically every 15 min, and pointing and focus were checked every 1 and 2 hrs respectively ensuring $\sim 1-3''$ accuracy. The APEX spectra were obtained in the classical ON-OFF mode, where the OFF at EQ 2000 coordinates 19:22:44.3, 14:05:50.0 shows no signal. The Fast Fourier Transform Spectrometer facility was used as a backend. For the IRAM observations, we used the VESPA autocorrelator, and the frequency-switching mode. All spectra were reduced using the CLASS package (Hily-Blant et al 2005) of the GILDAS software. Residual bandpass effects were subtracted using low-order (≤ 3) polynomials. Table 1 summarises the observed signals at each point and each observed transition.

CO emission is detected in the four observed transitions in all points. H^{13}CO^+ 1–0 emission is, on the contrary, detected towards three positions only: A, C and E. Finally, DCO^+ 1–0 emission is detected only towards the position E. The spectra towards the position E are shown in Fig.1. In general, there are two clouds in the line of sight, at different velocities v_{LRS} around 69 and around 73 km/s respectively. The line widths are similar in all points and transitions, about 3 km/s. The comparison of the ^{13}CO 2–1 observed with APEX and IRAM gives a direct measurement of the emitting sizes. Points B, C and E show extended ($\geq 28''$) emission, while in points A and D the sizes are about $20''$.

4. Analysis

4.1. Physical conditions and column densities

We used the non-LTE LVG code described in Ceccarelli et al. (2003), with the CO- H_2 collisional coefficients by Wernli et al. (2006) for the first 6 CO levels and the temperature range 5-70 K. We run a grid of models with temperatures between 10 and 50 K, densities between 10^3 and 10^5 cm^{-3} , C^{18}O column densities between 1×10^{14} and $4 \times 10^{16} \text{ cm}^{-2}$ and $^{13}\text{CO}/\text{C}^{18}\text{O}$ ratio between 5 and 15. For each point, we used the extent derived by the comparison of the ^{13}CO 2–1 line intensity obtained at APEX and IRAM telescopes, respectively. The values of the parameters minimising the χ^2 are reported in Tab. 2 (the range corresponds to $\chi^2=0.2$ contours). The H^{13}CO^+ column density has been derived by comparing the observed signals with non-LTE LVG computations using the collisional coefficients by Flower (1999) and the density and temperature derived from the previous step. The H^{12}CO^+ column density is then obtained by multiplying the $N(\text{H}^{13}\text{CO}^+)$ by 50 (Koo & Moon 1997). Note that the $[\text{DCO}^+]/[\text{HCO}^+]$ ratio very little depends on the actual gas temperature, for the range of temperatures considered here.

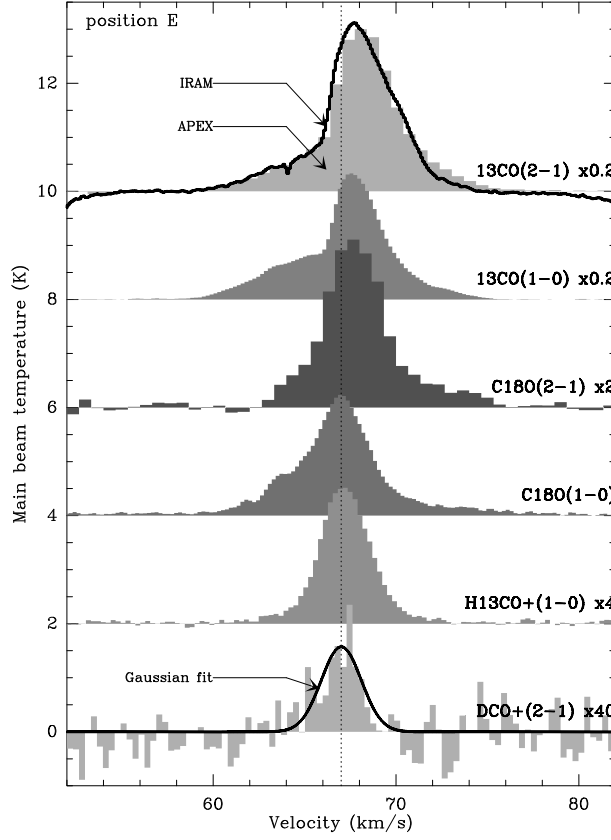


Fig. 1.— Observations towards position E. From top to bottom: ^{13}CO 2–1, ^{13}CO 1–0, C^{18}O 2–1, C^{18}O 1–0, H^{13}CO^+ 1–0 and DCO^+ 2–1. The signals are in main beam temperature K. The vertical line shows 67 km/s.

The clouds in the direction of points C1 and E have temperatures somewhat larger than 20 K, while the temperature is unconstrained in the other points. The densities are around 10^4 cm^{-3} in points C1, C2 and E, and unconstrained in the other points. The visual extinction A_V is few mag in points A and D, and it is larger than 10 mag in the other points. It is interesting and intriguing that points C1 and E have similar physical conditions but different column densities of HCO^+ and DCO^+ .

4.2. Ionization degree and CR Ionization rate

Using the analytical method mentioned in §1 (Eqs. 1 and 2 in CWTH98), from the $N(\text{DCO}^+)/N(\text{H}^{13}\text{CO}^+)$ ratio¹ we derive an extremely high ionization degree toward the point E, $x(e) \gtrsim 2 \times 10^{-5}$. This value is one or two orders of magnitude larger than those derived in other dark clouds by CWTH98. That point E is “special” with respect to the dark clouds of the CWTH sample is indeed already clear from the observed signals: in those clouds the DCO^+ 1-0 line intensity is of the same order of magnitude than the H^{13}CO^+ 1-0 line intensity (Butner et al. 1995), whereas we observed more than ten times lower DCO^+ 1-0 than the H^{13}CO^+ 1-0 line intensity. This is a hallmark that the ionization degree is much higher, and does not leave much of uncertainty on this conclusion. However, the analytical method is an oversimplification, especially for high ionization degrees, as more routes of HCO^+ formation become important in addition to the $\text{H}_3^+ + \text{CO}$ one.

In order to correctly evaluate the chemical structure of the cloud towards the point E, including the penetration of the interstellar (IS) UV photons and a (more) complete chemical network, we used the photo-dissociation region (PDR) models by Le Petit et al. (2006)². To help facilitate the discussion, Figure 2 shows the structure of a 20 mag cloud whose density is $1 \times 10^4 \text{ cm}^{-3}$, like point E, illuminated on the two sides by the IS UV field³ and with different CR ionization rates. As found by several previous studies, for a low value of ζ ($\lesssim 10^{-16} \text{ s}^{-1}$) and a low abundance of metals, the ionization through the cloud is governed by the UV photons penetration and depends on the abundance of carbon ($A_v \leq 2 \text{ mag}$) and sulphur ($2 \leq A_v \leq 4 \text{ mag}$), and on the CRs ionization deeper inside. The ionization at the interior of the cloud is low, 10^{-8} – 10^{-7} , in a phase called LIP (low ionization phase) in the literature (Pineau des Forêts et al. 1992). This situation is represented by the case $\zeta = 3 \times 10^{-17} \text{ s}^{-1}$ in Fig. 2. In general, as ζ increases the ionization in the cloud interior ($A_v \geq 2 \text{ mag}$) increases roughly quadratically until it reaches a critical point where it abruptly jumps to high values, in a phase called HIP (high ionization phase). The LIP/HIP transition is a result of the non-linear nature of the chemical network of molecular gas (e.g. Boger & Sternberg 2006; Rollig et al. 2007), which have been claimed to present a bistable nature (Le Bourlot et al. 1993). The spatial location of this transition depends upon various control parameters, among which the density, the abundance of He and metals, and the CR ionization rate (e.g. Wakelam et al. 2006). In practice, for a cloud of a given density, the LIP/HIP jump

¹We used the rate coefficients reported in database KIDA (<http://kida.obs.u-bordeaux1.fr/>).

²The code is available on the web site <http://pdr.obspm.fr/PDRcode.html>

³Higher values of the UV field would change the skin of the cloud only, so that we did not vary this parameter.

is governed by the metal abundances, specifically S, Si, Fe and Mg going inwards in the cloud, as metals are responsible for the (non-linear) charge exchange. As shown by Fig. 2, the zones closer to the cloud edge flip from LIP to HIP first, and the LIP/HIP jump moves further into the cloud with increasing ζ , until the whole cloud is in the HIP, regardless the metal abundances.

The HCO^+ abundance is affected by ζ (the larger the ζ the larger the HCO^+ formation rate) and by the presence of the HIP region (the larger the ionization degree the larger the HCO^+ destruction rate). In general, the HCO^+ abundance is roughly divided into three zones: in the skin of the cloud, it is very low because of the photo-dissociation by the UV photons, deeper in the cloud it increases but the high ionization in the HIP region keeps the HCO^+ abundance low, and at still larger A_v it increases, when eventually the gas jumps into the LIP.

The ratio $N(\text{CO})/N(\text{HCO}^+)$ of column densities, integrated over the 20 mag model cloud, is shown in Fig. 3. It decreases with ζ (as the HCO^+ abundance increases), until a critical point (at $\zeta \sim 1.0 - 1.3 \times 10^{-15} \text{ s}^{-1}$ depending on the metals abundance) where the whole cloud is in the HIP state and the HCO^+ abundance becomes very low all across the whole cloud. Note that for high metal abundances the cloud is always in the HIP state. As noted by Wakelam et al. (2006), the ionization distribution is bimodal with the metal abundances. In fact, the theoretical $N(\text{CO})/N(\text{HCO}^+)$ ratio either follows the high or the intermediate metal abundance curves of our Fig. 3.

The DCO^+ abundance follows qualitatively the behaviour of HCO^+ and the $\text{HCO}^+/\text{DCO}^+$ ratio across the cloud depends on the ionisation degree (~ 100 in the LIP and ≥ 1000 in the HIP zones, respectively). The dependence of the $N(\text{HCO}^+)/N(\text{DCO}^+)$ ratio as function of ζ is shown in Fig. 3. In practice, the values of $N(\text{CO})/N(\text{HCO}^+)$ and $N(\text{HCO}^+)/N(\text{DCO}^+)$ depend on the relative weight of the LIP-to-HIP zones in the integral over the cloud.

The comparison between the predicted $N(\text{CO})/N(\text{HCO}^+)$ and $N(\text{HCO}^+)/N(\text{DCO}^+)$ ratios with the values observed towards the point E provides a value of $\zeta \sim 1.0 - 1.3 \times 10^{-15} \text{ s}^{-1}$. The likely structure of the cloud in the point E is shown in Fig. 2. In practice, a large fraction of the cloud is the HIP state whereas the rest is in the LIP state. We stress, however, that, given the high non-linearity of the equations, the exact value of ζ which fits the observations depends on the details of the adopted model (Wakelam et al. 2006; Boger & Sternberg 2006). Regardless of these details, the modeling indicates a situation where high (HIP) and low (LIP) ionisation must be both present, to give the observed $\text{HCO}^+/\text{DCO}^+$ value which is an intermediate value of the two regions. The relative amounts of HIP/LIP may change with other control parameter values, but the result is that the line of sight we probe must contain both LIP and HIP. Finally, CR heat the cloud as they deposit energy so that the

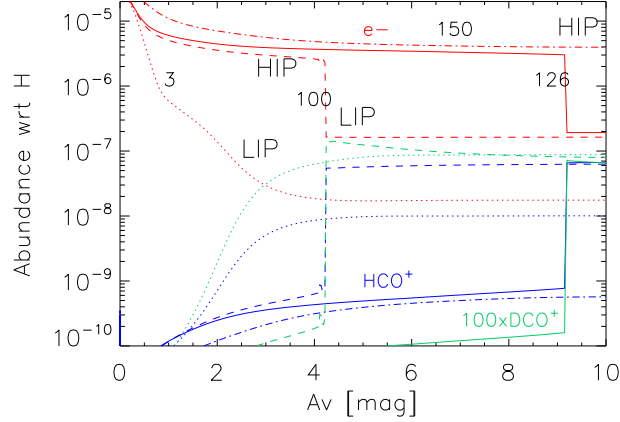


Fig. 2.— Structure of a 20 mag cloud of $1 \times 10^4 \text{ cm}^{-3}$ density illuminated by the IS UV field. Electrons (red curves), HCO^+ (blue curves) and $100\times\text{DCO}^+$ (green curves) abundances (with respect to H nuclei) for four different values of the CR ionization rate: 3 (dotted line), 100 (dashed line), 126 (solid line) and 150 (dashed-dotted line) $\times 10^{-17} \text{ s}^{-1}$. The LIP and HIP regions in the four cases are also marked (see text). The computations refer to the metal low abundances case. Only the 10 mag from the edge of the cloud are shown. Note that the $\zeta=126 \times 10^{-17} \text{ s}^{-1}$ case likely describes the situation towards point E.

relatively large value of the gas temperature (21–24 K) toward point E (Tab. 2) also favours the high ζ .

Finally, the lower limit to the $N(\text{HCO}^+)/N(\text{DCO}^+)$ towards point C1 suggests a value for ζ larger than in point E.

5. Conclusions

Our observations lead to two important conclusions:

- 1) The cloud towards the point E has a CR ionization rate $\zeta \sim 10^{-15} \text{ s}^{-1}$, i.e. enhanced by about a factor 100 with respect to the standard value (Glassgold & Dalgarno 1974). This is the first time that such an high ionization degree is measured in a dense molecular cloud. The fact that this cloud coincides with a TeV γ -rays source close to a SNR confornts the idea that it is irradiated by an enhanced flux of freshly formed low-energy CR. We have identified a location close to a CR accelerator with both enhanced low-energy CR ionization and high CR γ -ray emission, suggesting novel ways to study the acceleration and the diffusion of CR close to SN shocks.
- 2) The high low-energy CR flux induces the simultaneous presence of a region of high- and

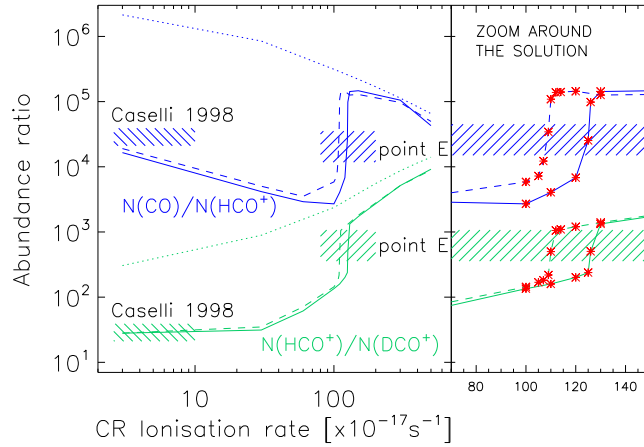


Fig. 3.— Observations against PDR model predictions: $N(\text{CO})/N(\text{HCO}^+)$ (blue) and $N(\text{HCO}^+)/N(\text{DCO}^+)$ (green) integrated over the 20 mag cloud. Three families of theoretical curves are reported with different metal abundances, following Wakelam et al (2006; see also CWTH98): high- (dotted), low- (solid) and intermediate- (dashed) abundances. The boxes show the observed values towards the point E and, for comparison, in the CWTH98 sample. The right panel shows a zoom around the solution. The red stars show the computed models.

low- ionization, called HIP and LIP in the literature. To our best knowledge, this is the first time that such a situation has been observed and offers the possibility to study in more detail the chemistry of the two states simultaneously. Therefore, a more general implication of this work is that TeV sources identified with SNRs interacting with molecular clouds are promising sites not only to study CR acceleration, but also to study unusual chemical conditions.

REFERENCES

- Abdo A.A., Ackermann M., Ajello M. et al. 2009, ApJ 706, L1
- Aharonian F.A. & Atoyan A.M. 1996, A&A 309, 917
- Aharonian F.A., Akhperjanian A.G., Bazer-Bachi A.R. et al. 2008, A&A 481, 401
- Albert J., Aliu E., Anderhub H. et al. 2007, ApJ 664, L87
- Boger G.I. & Sternberg A. 2006, ApJ 645, 314
- Butner H.M., Lada E.A., Loren R.B. 1995, ApJ 448, 207

- Caprioli D., Blasi P., Amato E. 2011, APh 34, 447
- Caselli P., Walmsley C.M., Terzieva R., Herbst E. 1998, ApJ 499, 234 (CWTH98)
- Ceccarelli C., Maret S., Tielens A.G.G.M., Castets A., Caux E. 2003, A&A 410, 587
- Fatuzzo M., Melia F., Todd E., Adams F.C. 2010, ApJ 725, 515
- Feinstein et al. 2009, AIPC 1112 54F
- Flower D.R. 1999, MNRAS 305, 651
- Gabici S., Aharonian F.A., Casanova S. 2009, MNRAS 396, 1629
- Glassgold A.E. & Langer W.D. 1974, ApJ 193, 73
- Guélin M., Langer W.D., Snell R.L., Wootten H.A. 1977, ApJ 217, L165
- Hayakawa S. 1952, PThPh 8, 571
- Hewitt J.W., Yusef-Zadeh F., Wardle M. 2008, ApJ 683, 189
- A.M. Hillas 2005, J. Phys. G: Nucl. Part. Phys., 31
- Hily-Blant P., Pety J. & Guilloteau S. 2005, CLASS Manual,
<http://www.iram-institute.org/medias/uploads/class-evol1.pdf>
- Le Boulrot J., Pineau des Forêts G., Roueff E., Schilke P. 1993, ApJ 416, L87
- Le Petit F., Nehm C., Le Boulrot J., Roueff E. 2006, ApJS 164, 506
- Kamae T., Karlsson N., Mizuno T., Abe T., Koi T. 2006, ApJ 647, 692
- Koo B-C., Kim K-T., Seward F.D. 1995, ApJ 447, 211
- Koo B-C. & Moon D-S. 1997, ApJ 485, 263
- Kundu M.R. & Velusamy T. 1967, AnAp 30, 59
- Montmerle T. 2010, ASPC 422, 85
- Padovani M., Walmsley C.M., Tafalla M., Galli D., Mller H.S.P. 2009, A&A 505, 1199
- Pineau des Forêts G., Roueff E., Flower D.R. 1992, MNRAS 258, 45
- Rollig M., Abel N.P., Bell T., Bensch F., Black J. et al. 2007, A&A 467, 187

Stecker F.W. 1971, *Nature* 234, 28

Wakelam V., Herbst E., Selsis F., Massacrier G. 2006, *A&A* 459, 813

Wernli M., Valiron P., Faure A., Wiesenfeld L., Jankowski P., Szalewicz K. 2006 *A&A* 446,
367

Table 1: Upper half table: Parameters of the observations. Lower half table: Observed positions with coordinates in J2000 and B1950 and line intensities main-beam temperatures (in K). Number in parenthesis are statistical uncertainties at the 1σ level. Lines in the position C show two separate velocity components. Notes:^aAPEX observations; ^bIRAM observations: note that the second velocity component of the point C is not detected because the line is at the border of the filter.

Species	Transition	Frequency (GHz)	Main beam efficiency	HPBW (arcsec)	Telescope	Journal	Res. (MHz)	T _{sys} (K)	
C ¹⁸ O	1–0	109.782	0.79	22	IRAM	May 2009	0.08	~ 100	
C ¹⁸ O	2–1	219.560	0.75	28	APEX	Dec 2008	0.5	~ 230	
¹³ CO	1–0	110.201	0.79	22	IRAM	May 2009	0.08	~ 100	
¹³ CO	2–1	220.399	0.55	12	IRAM	May 2009	0.08	~ 100	
¹³ CO	2–1	220.399	0.75	28	APEX	Dec 2008	0.5	~ 230	
H ¹³ CO ⁺	1–0	86.754	0.79	28	IRAM	May 2009	0.08	~ 100	
DCO ⁺	2–1	144.077	0.79	17	IRAM	May 2009	0.08	~ 100	
Position	Coordinates (J2000) (B1950)	<i>v</i> _{LSR}	¹³ CO		C ¹⁸ O		H ¹³ CO ⁺		DCO ⁺
			1–0	2–1 ^a	2–1 ^b	1–0	2–1	1–0	2–1
A	19:22:53.8 +14:15:44 19:20:35.9 +14:09:54	71.2	4.30(0.03)	6.20(0.05)	9.00(0.1)	0.30(0.03)	0.45(0.04)	0.040(0.006)	– (0.01)
B	19:22:31.0 +14:15:45 19:20:13.1 +14:09:57	69.0	7.60(0.04)	9.20(0.05)	17.85(0.2)	0.50(0.05)	1.10(0.04)	– (0.01)	– (0.02)
C1	19:22:21.3 +14:05:12	69.0	14.00(0.04)	19.40(0.10)	18.80(0.1)	2.00(0.03)	4.00(0.06)	0.23(0.01)	– (0.02)
C2	19:22:21.3 +14:05:12 19:20:03.2 +13:59:24	73.0	7.70(0.04)	14.80(0.10)	-	1.00(0.03)	2.70(0.06)	0.08(0.01)	– (0.02)
D	19:23:27.3 +14:16:24 19:21:09.4 +14:10:32	65.5	2.80(0.07)	4.20(0.07)	6.30(0.1)	0.15(0.02)	0.30(0.06)	– (0.007)	– (0.01)
E	19:23:08.0 +14:20:00 19:20:50.1 +14:14:09	67.0	11.70(0.10)	15.00(0.10)	15.6(0.1)	2.20(0.06)	4.20(0.06)	0.60(0.01)	0.040(0.006)

Table 2: Analysis results. $^{13}\text{CO}/[\text{C}^{18}\text{O}]$ ratio, temperature, density, C^{18}O and A_v (assuming $[\text{C}^{18}\text{O}]/[\text{H}_2]=2 \times 10^{-7}$ (Frerking et al. 1982) and the usual $N(\text{H}_2)=A_v \times 0.95 \times 10^{21} \text{ cm}^{-2} \text{ mag}^{-1}$), extent of the emitting region in arcsec, H^{13}CO^+ column density, and $[\text{DCO}^+]/[\text{H}^{13}\text{CO}^+]$ abundance ratio (assuming $[\text{HCO}^+]/[\text{H}^{13}\text{CO}^+]=50$) as derived by the analysis of the observed lines described in the text. The intervals account for the statistical uncertainty on the signals and on the physical parameters. To account for the uncertainty on the CO-to- A_v ratio, the A_v interval is increased by an additional 30%. Note that we run models with temperatures between 10 and 50 K and densities between 10^3 and 10^5 cm^{-3} so that the lower limits applies to these intervals only.

	$^{13}\text{CO}/[\text{C}^{18}\text{O}]$	Temp (K)	Density (10^3 cm^{-3})	$N(\text{C}^{18}\text{O})$ (10^{15} cm^{-2})	A_v (mag)	extent (arcsec)	$N(\text{H}^{13}\text{CO}^+)$ (10^{11} cm^{-2})	$[\text{DCO}^+]/[\text{HCO}^+]$
A	15	≥ 10	≥ 1	0.4–0.6	2–6	19	3–4	≤ 0.06
B	15	≥ 32	≥ 40	1.5–2.5	7–14	27	≤ 1	-
C1	15	23–28	6–20	3.9–4.1	16–24	≥ 28	7–9	≤ 0.002
C2	10	≥ 27	4–15	1.8–2.5	8–14	≥ 28	6–8	≤ 0.006
D	10	≥ 10	≥ 1	0.2–0.9	1–5	20	≤ 0.8	-
E	10	21–24	8–20	3.9–4.1	16–24	≥ 28	16–18	0.0012–0.0016